2009-01

Effect of thermal annealing treatments on the optical properties of rare-earth-doped AIN films

Journal of Physics D,Bristol,v. 42, n. 2, p. 025109-1-025109-7, Jan. 2009
http://www.producao.usp.br/handle/BDPI/49301

IOP PUBLISHING JOURNAL OF PHYSICS D: APPLIED PHYSICS

J. Phys. D: Appl. Phys. **42** (2009) 025109 (7pp) doi:10.1088/0022-3727/42/2/025109

Effect of thermal annealing treatments on the optical properties of rare-earth-doped AlN films

A R Zanatta

Instituto de Física de São Carlos – USP, São Carlos 13560-250, Brazil

Received 30 September 2008, in final form 24 October 2008
Published 18 December 2008
Online at stacks.iop.org/JPhysD/42/025109

Abstract

Aluminium–nitrogen (AlN) films doped with samarium, europium or ytterbium have been prepared by conventional radio frequency sputtering. Because of the deposition method and conditions the as-deposited films are amorphous with Sm, Eu or Yb concentrations at low 0.5 at%. After deposition the films were submitted to cumulative isochronal thermal annealing (TA) treatments and investigated by optical transmission spectroscopy, photo- (PL) and cathodoluminescence (CL) measurements. For comparison purposes one undoped AlN film was also prepared and investigated in detail. The experimental results indicate that (a) all samples exhibit PL and CL at room temperature, (b) the main spectral features present in the AlN samples are due to defect-related transitions (undoped film) or the rare-earth (RE) ions, (c) in both cases (undoped and Sm-, Eu- or Yb-doped films) the luminescence intensity scales with the temperature of TA and (d) for the present AlN samples, there is a clear relationship between their luminescence intensity and respective energy of optical bandgaps. Finally, the effect of TA on the excitation–recombination mechanisms involving the RE ions is presented and discussed.

(Some figures in this article are in colour only in the electronic version)

1. Introduction

Most of the studies on rare-earth- (RE-) doped compounds have been focused on the Er^{3+} ion and its infrared light emission at ∼1540 nm which is of great interest for telecommunication purposes [1]. This is because (just like any other RE ion) triply ionized Er species present sharp and well-defined optical emission at wavelengths that are practically insensitive to temperature and to the host material. The mechanisms behind the excitation of Er^{3+} ions and their subsequent (optical) recombination, however, are known to be highly susceptible to host details such as atomic structure and optical bandgap [2]. Accordingly, various different Er-doped compounds have been extensively investigated towards the achievement of more efficient phosphor materials and/or in the development of photonic devices. Actually, RE-doped semiconductor or dielectric compounds are expected to inspire not only the field of optical fibre-based telecommunications but to influence applications such as visible light-emitting diodes and color flat-panel displays, for example.

So far, RE-related visible light emission was achieved from the wide bandgap (WBG) materials BeN [3], AlN [4, 5], SiN [6], GaN [7] and GeN [8], for example, doped with many different RE ions. In addition to the possibility of extracting spectrally sharp RE-related luminescence from these matrices, it is well established that RE ions exhibit smaller luminescence quenching when inserted in WBG hosts. This phenomenon is usually attributed to the partial ionic character exhibited by WBG compounds, which influences both the energy and the localization of the electron–hole pairs generated during the luminescence process [2]. Within this context, and allied to their ability to work under extreme temperatures and hostile chemical environments, AlN films are promising candidates for a large number of applications in modern (micro-) electronics [9].

Stimulated by the above scenario this work reports on the optical properties of AlN films doped with Sm-, Eu- and Yb-ions. The films were prepared by the cosputtering method which allows the controllable insertion of RE species during deposition. With the purpose of probing the influence

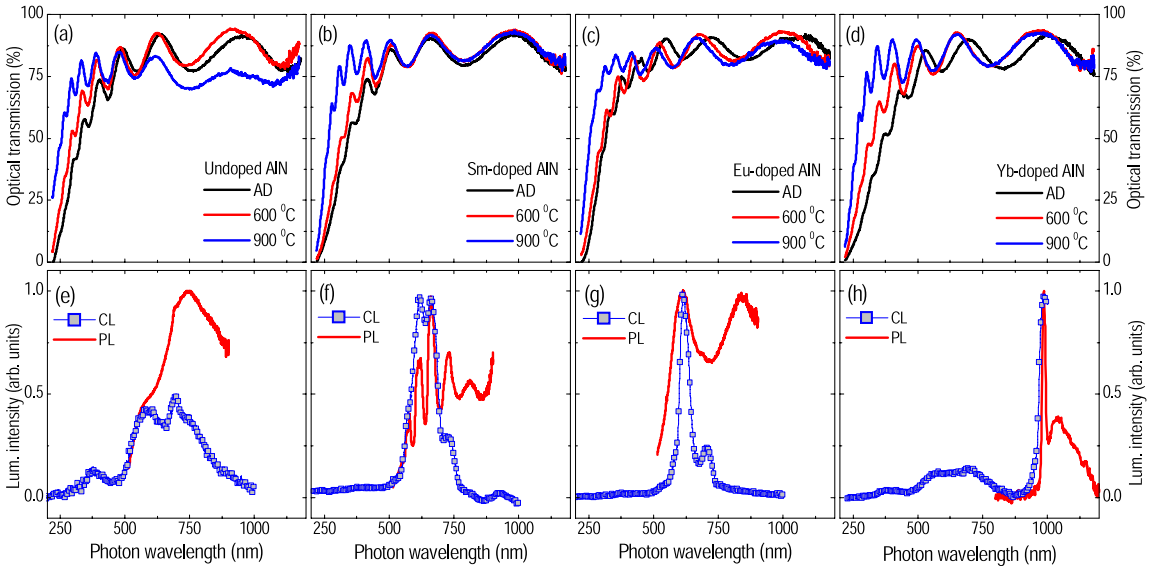

Figure 1. Optical transmission and PL and CL of AlN films: undoped (*a*) and (*e*), and doped with Sm (*b*) and (*f*), Eu (*c*) and (*g*) and Yb (*d*) and (*h*). The optical transmission measurements were obtained from films deposited on quartz substrates AD and after TA at 600 and 900 °C. Both PL and CL measurements were taken from AD films onto crystalline silicon substrates. All measurements were carried out at room temperature and corrected for system response. For comparison purposes the PL and CL spectra were normalized.

of thermal treatments on the optical properties and RE-related luminescence characteristics, all AlN samples were systematically investigated after TA up to 1050 °C.

2. Experimental details

Thin films of AlN were prepared by radio frequency (13.56 MHz) sputtering an Al target (99.999% pure) in an atmosphere of high-purity (99.999%) N_2 gas. The films, typically 500 nm thick, were deposited on crystalline Si and quartz substrates and the doping of AlN was achieved by partially covering the aluminium target with small pieces of Sm, Eu or Yb metal (99.9% pure). During deposition the substrates were kept at ∼150 °C. Based on the sputtering yield and on the relative target area occupied by Sm, Eu or Yb their atomic concentration was estimated to be at low 0.5 at% [10]. After deposition the films were submitted to isochronal (15 min long) TA treatments at 300, 450, 600, 750, 900 and 1050 °C under a continuous flow of argon.

The films were investigated by optical transmission and photo- (PL) and cathodoluminescence (CL) techniques. All measurements were conducted at room temperature in samples as-deposited (AD) and after thermal annealing (TA). Raman scattering spectroscopy (488.0 nm photons under backscattering geometry) was also performed in order to obtain some structural information. The UV–VIS optical transmission measurements were carried out in the ∼215–1050 nm wavelength range on films deposited on crystalline quartz substrates. The PL measurements employed an Ar^+-ion laser (488.0 nm photons and average power density of $\sim 3\,\mu W\,\mu m^{-2}$), whereas the CL experiments were achieved from a conventional scanning electron microscope (20 keV electrons and ∼80 nA) coupled to an optical detection system. With the exception of the PL measurements of the Yb-doped film (which employed a cooled Ge detector), all PL and CL signals were recorded by a Si-based charge-coupled device (CCD camera). Both Raman and luminescence experiments considered films deposited on crystalline silicon substrates.

3. Results

Raman scattering analyses indicate that the present AlN films are essentially amorphous even after TA at 1050 °C [11][1]. More sensitive structural measurements, provided by high-resolution transmission electron microscopy and electron diffraction measurements of similar RE-doped AlN films, however, suggest that the films consist of highly dispersed AlN nanocrystals (typically 10–20 nm large) embedded in an amorphous matrix [12].

The optical transmission spectra of some AlN films considered in this work (undoped, doped with Sm, Eu and Yb and after certain thermal treatments) are shown in the upper part of figure 1. The lower part of figure 1 illustrates the PL and CL spectra of AD AlN films as obtained at room temperature.

Because of different excitation mechanisms involving photons and electrons [6], the presence of a broad contribution in the PL spectra of figure 1 is noticeable. The experimental results also indicate that TA treatments affect both the PL and CL spectra (not shown): the spectral features remain essentially the same, but their overall luminescence intensity improves as the annealing temperature increases.

Following conventional thin film analysis [13], the optical transmission spectra of figure 1 were further processed

[1] Despite the low Raman activity involving Al–N bonds, Raman scattering spectroscopy is sensitive enough to detect the presence of AlN crystallites—as experimentally verified in AlN films deposited onto sapphire substrates by the ion-beam-assisted sputtering deposition method. Strictly, the amorphous character of the present AlN films, as indicated by Raman measurements, occurs essentially because of the deposition conditions (low temperature, low rf power and relatively high deposition pressure).

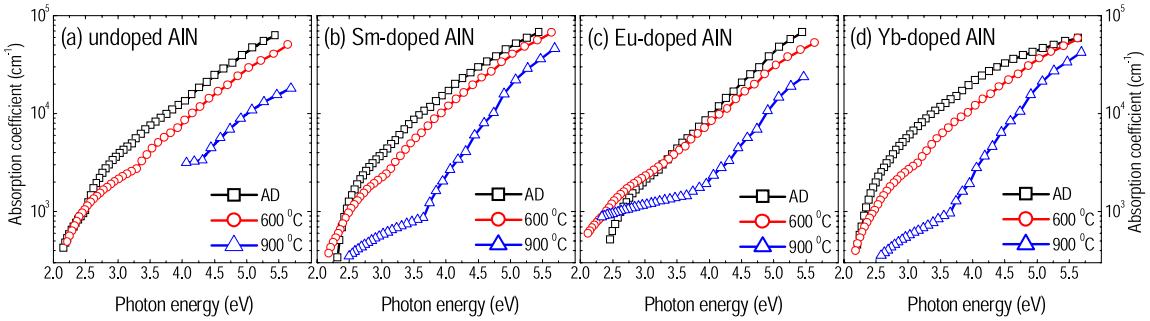

Figure 2. Optical absorption coefficient of AlN films AD and after TA at 600 and 900 °C: (*a*) undoped, (*b*) Sm-doped, (*c*) Eu-doped and (*d*) Yb-doped. The curves have been achieved after conventional thin film analysis of the transmission spectra of AlN films deposited on quartz substrates. The lines joining the experimental data are just guides to the eye.

to obtain the absorption coefficients (α) of all samples (figure 2). In addition to the absorption coefficient curves the method provides the thickness of the films as well as their corresponding optical bandgaps. According to this analysis all films are ∼500 nm thick, which is in perfect agreement with the values indicated by a quartz crystal thickness monitor during deposition. As the samples are annealed at increasing temperatures small variations can be verified in the sample thicknesses (500 ± 25 nm), but the main inconvenience stays in the development of pinholes in the films. The effect of these pinholes is evident from some transmission curves (undoped AlN film annealed at 900 °C in figure 1(*a*) and Eu-doped AlN annealed at 900 °C in figure 1(*c*), for example) and prevents the precise evaluation of the optical constants.

4. Discussion

It is well established that the ultimate properties of any synthetic material depend not only on its atomic structure and chemical composition but also on its preparation method and conditions. This is particularly true for non-crystalline or amorphous (a-) films for which several experimental techniques have been considered to produce high-quality materials [14, 15]. Likewise, post-deposition treatments such as TA, for example, can induce considerable changes in the optical–electronic–structural properties of a-films and deserve special attention. Most of these aspects can be efficiently probed by means of optical spectroscopic techniques which, in addition, are non-destructive and relatively fast.

4.1. Optical absorption

Different from the optical processes that occur in crystalline materials, the optical absorption exhibited by non-crystalline or a-films is highly influenced by the presence of localized electronic states near the conduction (CB) and valence band (VB) edges. These (band-tail) states arise mainly due to the intrinsic atomic disorder characteristic of a-materials, but can also originate from the presence of charged defects, impurities, etc [16]. As a consequence, the optical absorption of a-films is commonly divided into three main regions [14, 15].

(a) The intrinsic (or Tauc's) region (absorption coefficient $\alpha \geqslant 10^4\,\mathrm{cm}^{-1}$)—involving transitions between extended electron states, where the optical absorption is essentially determined by the convolution of the VB and CB states and by the matrix element for optical transitions,
(b) the exponential (or Urbach's) region ($\sim 10^2 \leqslant \alpha \leqslant 10^4\,\mathrm{cm}^{-1}$)—typically taken as a measure of the disorder and that corresponds to transitions between extended and band-tail states and
(c) the low-absorption (or defect-related) region ($\alpha \leqslant 10^2\,\mathrm{cm}^{-1}$)—associated with transitions between tail states and deep defects.

In fact, the occurrence of these different absorption regions prevents the accurate evaluation of optical bandgaps in a-materials for which several experimental approaches are currently in use. The simplest one is to consider the optical bandgap as the energy corresponding to absorption coefficients equal to 10^3 or $10^4\,\mathrm{cm}^{-1}$ denoting the E_{03} and E_{04} bandgaps, respectively. Another usual definition (the so-called Tauc's bandgap E_{Tauc}) is based on the complete relaxation of the electron wavevector selection rules (random-phase approximation) and on the assumption that the CB and VB are parabolic-shaped [$\alpha(E) \propto (E - E_{\mathrm{Tauc}})^2$] [17]. These experimental approaches not only provide a good measure of the optical bandgap of non-crystalline or a-films but can be very helpful in the identification and study of the different optical–electronic–structural processes occurring in these materials [14].

The optical analysis of the present AlN films comprised the determination of the E_{04}, E_{Tauc} and E_{03} bandgaps as well as their evolution as the TA treatments advanced (figure 3). For comparison purposes, the E_{03} and E_{04} optical bandgaps of nano-crystalline AlN films prepared by either reactive sputtering [18] or impulse plasma assisted chemical vapour deposition [19] are shown in figure 3(*a*).

As can be seen from figure 3, thermal treatments at increasing temperatures induce considerable changes in the optical bandgap of all AlN films. A part of them can be summarized as follows: (a) all samples present different values of E_{04}, E_{Tauc} and E_{03}, but they do not seem to be influenced directly by doping with Sm, Eu or Yb, (b) an optical bandgap widening of (at least) 1 eV can be verified after thermal annealing the films at 900–1050 °C and (c) the main effect of TA is to reduce the density of tail-states, as suggested by the optical bandgap widening at increasing

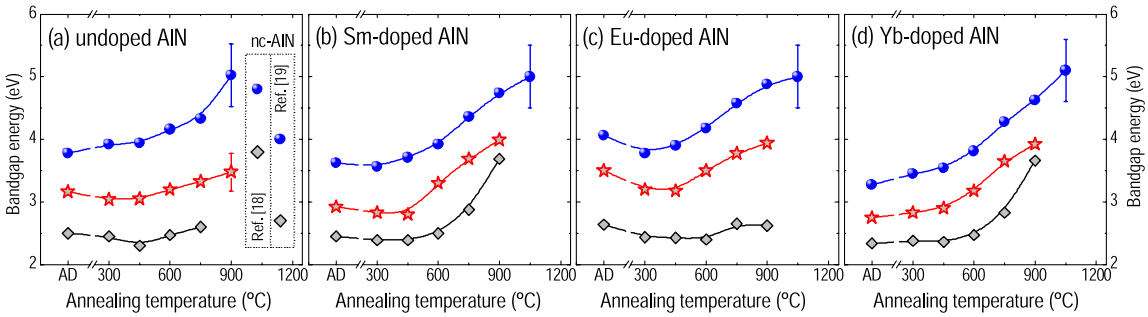

Figure 3. E_{04} (circles), E_{Tauc} (stars) and E_{03} (diamonds) optical bandgaps of AlN films ((*a*) undoped, (*b*) Sm-doped, (*c*) Eu-doped, and (*d*) doped with Yb), AD and after TA at 300, 450, 600, 750, 900 and 1050 °C. The lines joining the experimental data are just guides to the eye. The E_{03} and E_{04} values of nano-crystalline (nc-) AlN films [18, 19] are also shown for comparison.

temperatures. In this last case, it is believed that TA can promote some structural rearrangement and/or the diffusion of atomic nitrogen favouring the development of a less disordered AlN matrix. This is corroborated by the luminescence results as will be shown in sequence. Finally, the difference between the optical bandgaps exhibited by undoped AlN samples (figure 3(*a*)) simply because of the deposition method and atomic structure is remarkable.

4.2. Optical emission

Depending on the chemical–structural characteristics of the solid host, RE species can exist under the trivalent and/or divalent ionic forms [20, 21]. As a matter of fact, Sm, Eu and Yb are within the lanthanides that more frequently exhibit this behaviour. Therefore, besides the study of RE-doped AlN films as new luminescent materials, and the influence of TA on their optical properties, this work was also intended to test the presence of divalent RE ions in these samples. Because RE^{3+} and RE^{2+} ions can coexist in certain solid hosts, experimental methods such as PL and CL are required to detect their presence at very low concentration levels. Whereas the basics behind PL and CL spectroscopies are very similar, their main differences rely on the means and energy range of excitation [22].

CL excites by energetic electrons (typically in the keV range), which induces luminescence via various different routes: band-related, impurity- (or doping-) related, through exciton coupling, surface plasmon decay, etc. During a CL experiment, for example, the incoming fast electron represents a momentum of applied charge to the solid and demands dissipation of excess energy. As a result, CL is able to generate great densities of hot electron–hole pairs due to the incoming negatively charged electrons. PL, on the contrary, utilizes uncharged particles (photons) corresponding to the ultraviolet–visible–infrared regions of the electromagnetic spectrum. In this case, the energies involved in the whole process are considerably lower and each absorbed photon is able to produce only one excited electron. Furthermore, it is important to mention that, due to the excitation energies typically involved in luminescence experiments, PL is able to perform (quasi-) resonant excitation of the RE ions, while CL is almost exclusively based on band-to-band excitation.

The PL and CL spectra of some AlN films, AD and at room temperature, are already presented in figure 1. It is clear from the figure that all films exhibit luminescence, which can be either RE-related (figures 1(*f*)–(*h*)) or due to the AlN matrix (figure 1(*e*)). According to the experimental results, light emission from the undoped film takes place through broad contributions at ∼375, 580 and 730 nm, their relative intensities being sensitive to the annealing temperature (not shown). These emission bands are generically attributed to transitions involving point defects [23–25]: (a) in the ∼275–450 nm wavelength range, due to N- or Al-vacancies (V_N or V_{Al}) or to antisite Al defects (Al_N), and (b) in the ∼670–880 nm range, due to N_{Al}. Also, the high reactivity of aluminium to oxygen cannot be ignored and some of the above transitions could be due to (or influenced by) its unintentional presence.

A sketch illustrating the energy levels between the VB and CB of AlN, the forms of energy excitation (essentially PL and CL) and respective radiative recombination paths is shown in figure 4. For the undoped AlN sample (figure 4(*a*)), the energy levels refer both to point defects (V_N, V_{Al}, Al_N and N_{Al}) and to the morphological disorder (tail-states) present in amorphous or partially crystallized films. As the thermal treatment advances, a part of these defects is suppressed inducing clear changes in all optical–electronic processes (see figures 2(*a*) and 3(*a*), for example). This phenomenon can be attributed to some atomic diffusion and/or structural reordering which substantially reduce the number of sub-bandgap absorption centres.

A very similar reasoning applies to the RE-doped AlN films where the TA treatments also act inhibiting the non-radiative paths, with consequent improvement in both optical absorption and emission processes. While the optical absorption of all AlN samples considered in this work are similar—specially because of the low content of RE impurities—their light emission results need further discussion. Most of the luminescence observed from the RE-doped AlN samples originates from transitions associated with Sm^{3+} (and Sm^{2+}), Eu^{3+} or Yb^{3+} ions. In this case, the main luminescence features present in figures 1(*f*)–(*h*) are associated with the following electronic transitions [26].

(i) *Sm^{3+} and Sm^{2+} ions (figure 4(b)).* In the visible energy range three main contributions appear: $^4G_{5/2} \rightarrow {}^6H_{5/2}$ (at ∼575 nm), $^4G_{5/2} \rightarrow {}^6H_{7/2}$ (at ∼615 nm) and $^4G_{5/2} \rightarrow {}^6H_{9/2}$ (at ∼664 nm). At ∼730 nm the signal corresponds to the

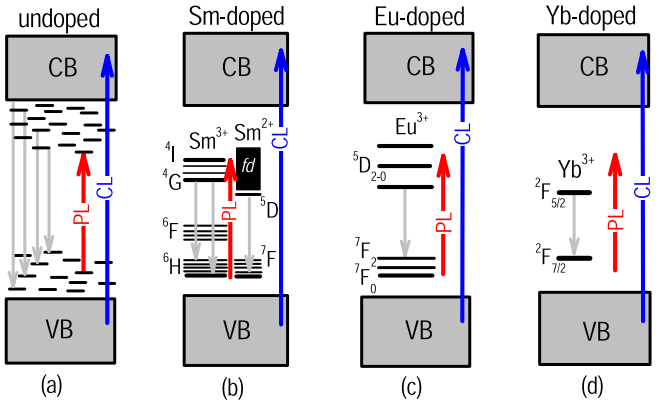

Figure 4. Simplified diagram illustrating the CB and VB of AlN films as well as the energy levels associated with the presence of defects and RE ions in the AlN matrix. PL and CL (upward arrows) stand for the excitation provided by photons (488.0 nm) and electrons (20 keV), respectively. The downward arrows denote some of the luminescence signals that can be observed in the present AlN samples. For clarity reasons the defects typically found in the undoped AlN film were omitted in (*b*), (*c*) and (*d*). The arrangement of the energy levels (between VB and CB) and the upward and downward arrows are only illustrative and are not to scale.

superposition of the $^4G_{5/2} \rightarrow {}^6H_{11/2}$ transition due to Sm^{3+} ions and the $^5D_0 \rightarrow {}^7F_0$, $^5D_0 \rightarrow {}^7F_1$ and $^5D_0 \rightarrow {}^7F_2$ transitions due to Sm^{2+}. The infrared emission at ∼814 nm is ascribed to the $^5D_0 \rightarrow {}^7F_4$ transition and is exclusively related to Sm^{2+} ions. The broad PL contribution that takes place in the ∼700–1000 nm wavelength range can be indistinctly associated with the $4f^5 5d^1 \rightarrow 4f^6$ transitions (typical of Sm^{2+} ions) or with the luminescence due to the AlN matrix (figure 1(*f*)).

(ii) *Eu^{3+} ions (figure 4(c)).* Most of the CL features present in figure 1(*g*) refer to transitions involving the ^5D and ^7F electron states: from the $^5D_{1,2}$ state to the ^7F_J manifold (weak signal at ∼545 nm), $^5D_0 \rightarrow {}^7F_2$ (at ∼615 nm) and $^5D_0 \rightarrow {}^7F_4$ (at ∼710 nm). Although light emission due to Eu^{2+} ions ($4f^6\ 5d^1 \rightarrow 4f^7$ transition) has been found in the ∼600–700 wavelength range, it usually takes place in the violet–green region [27, 28] and is clearly absent in the present Eu-doped AlN samples. In addition to a considerable background, the PL spectrum also exhibits the $^5D_0 \rightarrow {}^7F_2$ transition (at ∼615 nm) and some light emission at approximately 840 nm. The infrared contribution at 840 nm does not refer to Eu^{3+} (or Eu^{2+}) ions and, considering the photon excitation energy (sub-bandgap and out of resonance), it is tentatively ascribed to some defect or unintentional contamination present in the AlN matrix.

(iii) *Yb^{3+} ions (figure 4(d)).* In its $4f^{13}$ electron configuration, Yb^{3+} ions only have the $^2F_{7/2}$ and $^2F_{5/2}$ spin–orbit manifolds. The optical emission processes involving these two energy levels usually take place at ∼980 nm and exhibit many vibronic sidebands [27, 29], in perfect agreement with the spectra of figure 1(*h*). In its $4f^{14}$ electron configuration, however, Yb^{2+} ions present light emission in the ultraviolet–green spectral region that is usually broad and structureless, as expected for f–d transitions [28]. Whereas the signal at ∼980 nm (and at higher wavelengths) corresponds to $^2F_{5/2} \rightarrow {}^2F_{7/2}$ due to Yb^{3+} ions, the origin of the emissions verified in the ∼500–750 nm range and at ∼380 nm are uncertain. At this time, they can be ambiguously associated with the transitions observed in the undoped AlN sample (figure 1(*e*)) or to the presence of Yb^{2+} ions.

Indeed, the study of RE^{2+} ions in solid matrices is quite an exciting field. According to the literature, they are hardly seen in oxygen-rich environments. The only exception is the Eu^{2+} ion that can be achieved without great difficulty (provided that in a convenient atomic environment) and in a higher fraction than Eu^{3+}.

The diagram of figure 4 also shows some possible excitation routes when using 488.0 nm (PL) or 20 keV (CL) sources. Considering the bandgap of the AlN samples (in the order of 4–5 eV), it is clear that 20 keV electrons only provide band-to-band excitation. The electron–hole pairs generated during the CL experiments transfer their energy to the tail- or defect-states present in the AlN matrix, from where they can recombine radiatively (figure 1(*e*)) and/or transfer their energy to the Sm-, Eu- or Yb-ions (figures 1(*f*)–(*h*)). In both cases (AlN- and RE-related light emission), the luminescence signal is improved by TA which acts by reducing the energy losses due to non-radiative recombination processes. Excitation with 488.0 nm photons, on the contrary, only takes place at states inside the bandgap of AlN and a considerable energy transfer from the tail-states to the RE ions is expected to occur. Based on the energy levels diagram of figure 4(*b*) it is reasonable to assume, however, that most of the photons at 488.0 nm are absorbed by the $^4I_{9/2}$ energy level of the Sm^{3+} ions and by the $4f^5 5d^1$ band of the Sm^{2+} ions. Such a quasi-resonant excitation mechanism has already been observed in many other RE-doped films and seems to be very efficient [3, 5, 6, 8, 10].

The progress of some of the above discussed luminescence signals has been investigated as a function of the annealing temperature (figure 5). Despite small deviations in the relative luminescence intensity, the experimental results indicate an overall improvement of both PL and CL intensities as the thermal treatments advance. Due to the smaller excitation energy, and comparatively straightforward excitation–recombination mechanisms, the effect of thermal treatments will be discussed based only on the PL results. Furthermore, since all PL transitions display a similar dependence with the annealing temperature, figure 5 contains the PL intensity at particular wavelengths: ∼580 for the undoped AlN, ∼620 nm for the Sm-doped, ∼615 nm for the Eu-doped and ∼985 nm for the Yb-doped sample.

Compared with the AD films, the RE-doped AlN samples display an improvement of about one order of magnitude in the PL intensity (I_{PL}) when annealed at increasing temperatures (figures 5(*b*)–(*d*)). The effect of TA on the E_{04} optical bandgap of the AlN samples is also noteworthy and is shown in figure 5 for comparison purposes.

The changes experienced by both E_{04} and I_{PL} are attributed to the decrease in tail-states present in the AlN samples. In the case of the E_{04} optical bandgap the suppression of tail-states induces a reduction in defect-related absorption processes and are at the origin of the observed bandgap widening [14, 15, 30]. Likewise, the improvement in I_{PL} occurs because of a decrease in the number of non-radiative

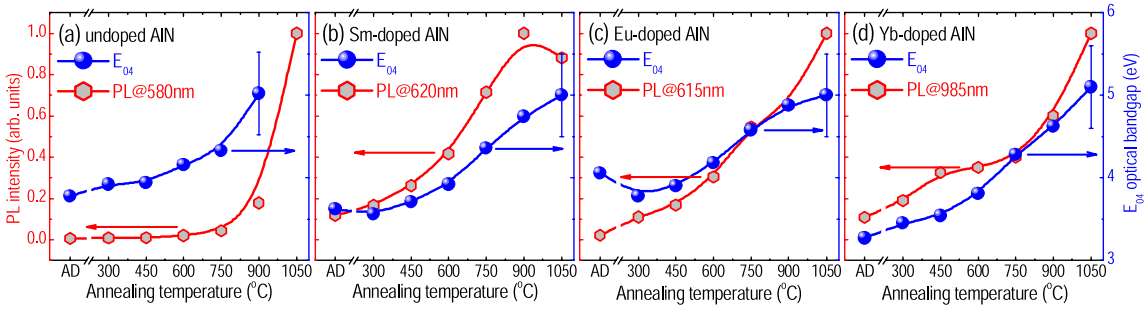

Figure 5. PL intensity (left-hand axis) and E_{04} optical bandgap (right-hand axis) of AlN films as a function of the annealing temperature. For comparison purposes the PL data were normalized and takes into account the maximum intensity at the photon wavelengths indicated in the figure. The lines joining the experimental data are just guides to the eye. AD stands for as-deposited.

transitions and/or in the probability of re-absorption or back-transfer processes [2]. In fact, RE^{3+} ions are known to be excellent recombination centres which effectively compete with other non-radiative processes taking place in amorphous or non-crystalline hosts. Finally, the effect of the tail-states on the PL intensity seems to be even more severe in the undoped AlN sample where a significant I_{PL} enhancement is verified only after TA at 900 and 1050 °C.

5. Concluding remarks

Amorphous AlN films doped with Sm, Eu or Yb have been prepared by conventional radio frequency sputtering in an atmosphere of pure nitrogen. After deposition the films were submitted to cumulative thermal treatments and their optical–electronic characteristics were investigated by means of different spectroscopic techniques. The AlN films doped with Sm, Eu or Yb exhibit characteristic RE-related light emission after excitation with 488.0 nm photons or 20 keV electrons. According to the Raman measurements, the films remain amorphous even after annealing at 1050 °C. At this point, it is not possible to exclude the existence of small AlN crystallites highly dispersed in the amorphous AlN matrix, but they certainly do not interfere in most of the optical–electronic properties of the films under study.

A detailed examination of the experimental results allowed the identification of all luminescence features either due to the RE ions or the AlN matrix. PL and CL spectra present differences that are expected because the energetics involving photon or electron excitation are very different. According to the experimental data it is reasonable to assert that RE^{3+} ions are excited through carrier-mediated processes when electrons are used. The excitation of the RE ions by 488.0 nm photons, on the other hand, involves defect-related absorption with subsequent energy transfer (AlN matrix → RE ion) or, in the case of the Sm^{3+} and Sm^{2+} ions, quasi-resonant energy excitation.

The optical absorption of the present AlN samples is greatly influenced by the TA treatments, which essentially act suppressing tail- or defect-states. Consistently, the luminescence intensity experiences a significant improvement as the thermal treatments advance. In fact, most of the observed luminescence enhancement is believed to be directly related to the suppression of tail-states and consequent reduction in the probability of non-radiative recombination.

Acknowledgments

The author is indebted to Dr R Weingaertner (University of Erlangen- Germany) and to MSc F Ferri (USP- Brazil) for the CL measurements and assistance with the optical analyses, respectively. The Brazilian agencies FAPESP and CNPq are also acknowledged for providing financial support.

References

[1] For a review on the subject see, for example, Kenyon A J 2002 *Prog. Quantum Electron.* **26** 225
[2] Zanatta A R 2003 *Appl. Phys. Lett.* **82** 1395
[3] Zanatta A R, Richardson H H and Kordesch M E 2007 *Phys. Status Solidi (RRL)* **1** 153
[4] Kurumurugan K, Chen H, Harp G R, Jadwisienczak W M and Lozykowski H J 1999 *Appl. Phys. Lett.* **74** 3008
[5] Ribeiro C T M, Alvarez F and Zanatta A R 2002 *Adv. Mater.* **14** 1154
[6] Zanatta A R, Ribeiro C T M and Jahn U 2001 *Appl. Phys. Lett.* **79** 488
[7] Steckl A J and Zavada J M 1999 *Mater. Res. Soc. Bull.* **24** 16
[8] Zanatta A R and Ribeiro C T M 2004 *J. Appl. Phys.* **96** 5977
[9] See, for example, Gil B (ed) 1998 *Group III-Nitride Semiconductor Compounds* (Oxford: Clarendon)
[10] Zanatta A R, Ribeiro C T M and Jahn U 2005 *J. Appl. Phys.* **98** 093514
[11] See, for instance, Ribeiro C T M, Alvarez F and Zanatta A R 2002 *Appl. Phys. Lett.* **81** 1005
[12] Weingaertner R, Erlenbach O, Winnacker A, Welte A, Brauer I, Mendel H, Strunk H P, Ribeiro C T M and Zanatta A R 2006 *Opt. Mater.* **28** 790
[13] Swanepoel R 1983 *J. Phys. E: Sci. Instrum.* **16** 1214 and references therein
[14] See, for example, Mott N F and Davis E A 1979 *Electronic Processes in Non-Crystalline Materials* (Oxford: Clarendon)
[15] Street R A 1991 *Hydrogenated Amorphous Silicon* (Cambridge: Cambridge University Press)
[16] Zanatta A R and Chambouleyron I 1996 *Phys. Rev.* B **53** 3833 Zanatta A R, Mulato M and Chambouleyron I 1998 *J. Appl. Phys.* **84** 5184 and references therein
[17] Tauc J, Grigorocivi R and Vancu A 1966 *Phys. Status Solidi* **15** 627
[18] Abe K, Nonomura S, Kobayashi S, Ohkubo M, Gotoh T, Nishio M, Niita S, Okamoto S and Kanemitsu Y 1998 *J. Non-Cryst. Solids* **227–230** 1096

[19] Siwiec J, Sokolowska A, Olszyna A, Dwilinski R, Kaminska M and Hrabowska J K 1998 *Nano-Struct. Mater.* **10** 625
[20] Moeller T 1973 *The Chemistry of the Lanthanides* (Exeter: Pergamon)
[21] Blasse G and Grabmaier B C 1994 *Luminescent Materials* (Berlin: Springer)
[22] See, for instance, Yacobi B G and Holt D B 1999 *Cathodoluminescence Microscopy of Inorganic Solids* (New York: Plenum) and references therein
[23] Tansley T L and Egan R J 1992 *Phys. Rev.* B **45** 10942
[24] Sun J, Wu J, Ling H, Shi W, Ying Z and Li F 2001 *Phys. Lett.* A **280** 381
[25] Senawiratne J, Strassburg M, Dietz N, Haboeck U, Hoffmann A, Noveski V, Dalmau R, Schlesser R and Sitar Z 2005 *Phys. Status Solidi* c **2** 2774
[26] Dieke G H 1968 *Spectra and Energy Levels of Rare-Earth Ions in Crystals* (New York: Wiley Interscience)
[27] Henderson B and Imbusch G F 1989 *Optical Spectroscopy of Inorganic Solids* (Oxford: Clarendon)
[28] Dorenbos P 2003 *J. Phys.: Condens. Matter* **15** 575
Dorenbos P 2003 *J. Lumin.* **104** 239
[29] Buchanan R A, Wickersheim K A, Pearson J J and Herrmann G F 1967 *Phys. Rev.* **159** 245
[30] de Oliveira V I, Freire F L Jr and Zanatta A R 2006 *J. Phys.: Condens. Matter* **18** 7709